

Lumos: Democratizing SciML Workflows with L0-Regularized Learning for Unified Feature and Parameter Adaptation

Shouwei Gao[†], Xu Zheng^{*}, Dongsheng Luo^{*}, Sheng Di[‡], Wenqian Dong[†]

[†]Oregon State University, ^{*}Florida International University, [‡]Argonne National Laboratory

Abstract—The rapid growth of scientific machine learning (SciML) has accelerated discovery across diverse domains, yet designing effective SciML models remains a challenging task. In practice, building such models often requires substantial prior knowledge and manual expertise, particularly in determining which input features to use and how large the model should be. We introduce Lumos, an end-to-end framework based on L0-regularized learning that unifies feature selection and model pruning to democratize SciML model design. By employing semi-stochastic gating and reparameterization techniques, Lumos dynamically selects informative features and prunes redundant parameters during training, reducing the reliance on manual tuning while maintaining predictive accuracy. We evaluate Lumos across 13 diverse SciML workloads, including cosmology and molecular sciences, and demonstrate its effectiveness and generalizability. Experiments on 13 SciML models show that Lumos achieves 71.45% parameter reduction and a 6.4× inference speedup on average. Furthermore, Distributed Data Parallel (DDP) training on up to eight GPUs confirms the scalability of Lumos.

I. Introduction

Scientific applications span a wide spectrum of computational tasks aimed at solving complex, real-world problems. However, these tasks are often very computation-intensive due to the high complexity of simulation algorithms and data analysis. Scientific Machine Learning (SciML) models can address these challenges with their highly accurate modeling capabilities on complex (non-)linear scientific datasets, concurrent computation patterns on AI/ML blocks, and less sensitivity to processor architectures. Recent studies demonstrate that integrating SciML models with traditional HPC applications can achieve significant speedups of 10^3 or more [1]–[3]. SciML has also led to breakthroughs in diverse fields, gaining widespread adoption such as improving predictions of extreme weather events [4] in climate science; enhancing gene expression analysis [5] in genomics; and accelerating the identification of potential drug candidates [6] in drug discovery, respectively. Meanwhile, SciML is undergoing a paradigm shift with the advent of foundation models like AlphaFold-3 [7], PanGu- Σ [8], and ClimaX [9], which are pretrained models on large and general datasets and can be adapted to various downstream tasks through fine-tuning [10]–[22]. These foundation models has strong generality due to trained from boarder dataset, and cost-efficient with less training steps.

However, in both mainstream SciML workflows, the efficiency of scientific input features and SciML model parameters remains poorly studied. Figure 1 showcases

the two scenarios (S1 and S2) present critical and shared challenges in the designing pipelines.

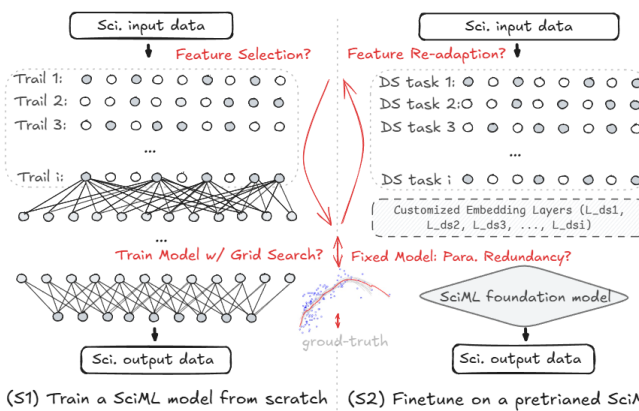


Fig. 1: (S1) Training from scratch: domain scientists must select physics-informative scientific input features and co-design the model architecture and parameters, often relying on costly grid search and ad hoc heuristics. (S2) Fine-tuning a foundation model: the pretrained backbone is fixed, and adaptation is achieved by re-mapping input features and adjusting subsets of parameters. Both workflows face common bottlenecks in feature efficiency and model/parameter efficiency, motivating the development of unified frameworks such as Lumos.

In the case of (S1) training from scratch, domain scientists must decide the importance of scientific input features in the training of the SciML model. Identifying the most relevant input features is often difficult due to the complex, high-dimensional nature of scientific systems, where intricate variable interactions and hidden dependencies are common. Selecting salient features from a vast array of potential inputs is crucial for achieving accurate and efficient approximations [23], yet existing feature selection methods often suffer from low explainability, neglect of output quality, or excessive computational overhead (see Section II.1). In practice, this problem is compounded by the need to co-design feature choices with the model architecture and hyperparameter search. Traditional training practices frequently resort to exhaustive grid search across architectures, parameters, and feature subsets [24], [25]. However, such brute-force approaches are labor-intensive and may result in significant redundancy, as not all input dimensions contribute equally to the predictive accuracy of the model. Also, this inefficiency is even worse when the model size grows and the parameter space becomes

prohibitively large, making scalability a critical issue.

In contrast, (S2) fine-tuning a pre-trained foundation model shifts the burden from training an entire model to re-adapting customized embedding layers for the specific dataset at hand (based on the needs of downstream tasks). Here, the central question is not only which features are most relevant, but also how to best re-map scientific input descriptors into the latent representation space of the foundation model. While foundation models provide strong generalization ability, naïve adaptation can still result in parameter inefficiencies and performance bottlenecks, particularly when downstream datasets are small, noisy, or domain-shifted. With fixed and large pretrained weights, these models risk over-parameterization, leading to overfitting, high energy costs, and inference delays. Moreover, over-complex models consume large amount of memory and computational resources, conflicting with real-time simulation or analysis needs in scientific domains such as high-energy physics, where computational bottlenecks may hinder the detection of rare events [26]. Existing efficiency strategies, such as model compression, provide partial solutions but still face major limitations (see Section II.2).

At their core, both scenarios highlight two intertwined and insufficiently addressed challenges: (i) feature efficiency, that determines which scientific input features are most relevant and how to adapt them effectively across tasks and domains; ii) model architecture and parameter efficiency, that decides how to allocate, adapt, or prune parameters to balance accuracy with computational cost, particularly under the constraints of heterogeneous scientific datasets.

To tackle these challenges, we propose Lumos, an end-to-end, self-guided framework that applies L0-regularized learning that folds scientific feature selection and parameter optimization (such as structure pruning) into a traditional SciML training or fine-tuning pipeline. Lumos enables domain scientists to construct compact but efficient models without labor-intensive manual intervention or domain-specific heuristics. By automating these optimization steps, Lumos facilitates both from-scratch surrogate training and fine-tuning of foundation models, increasing stakeholders’ confidence in deploying SciML in real-world scientific workflows.

This paper makes the following contribution:

- We propose Lumos, a unified framework that can conduct feature selection and parameter pruning simultaneously for SciML models. Lumos leverages learnable and differentiable semi-stochastic neuron gates to enable dynamic optimization during training or fine-tuning.
- Lumos introduces structural consistency mapper functions to track and reconciles architectural transformation to maintain the alignments of weights, activation tensors (such as KV tensors in attention layer)

and outputs across SciML layers when conducting feature and parameter pruning.

- Lumos can be seamlessly integrated into existing SciML training or fine-tuning pipelines within their training phase, performing on-the-fly feature and parameter selection with negligible overhead. Across the 13 evaluated SciML models, the additional gate parameters introduced by Lumos only take about 3% on average. We demonstrate its effectiveness and generality across five representative layer types including fully connected layers, convolutional layers, Graph Isomorphism Network (GIN) layers, Graph Convolutional Network (GCN) layers, and attention layers, covering diverse scientific domains such as cosmology, molecular science, and materials research.

II. Background and Related Work

A. Feature Selection

Feature selection methods can be divided into three categories [27]: ❶ Filtering [28] evaluates the correlation between features through statistical measurement. Common techniques include Pearson’s correlation coefficient [29], Chi-square test [30], and Mutual Information (MI) [31]. These methods rank features based solely on their intrinsic characteristics in relation to the target variable, making them computationally efficient. However, because they do not consider interactions between features and the model, filtering methods usually overlook complex dependencies within the data. ❷ Wrapper methods such as forward selection [32], backward elimination [33], or greedy search strategies [34], typically utilize iterative processes to select a subset of features. An example is the LM-FM framework proposed by Korfi et al. [35], which employs Local Maximization (LM) and Floating Maximization (FM) stages to optimize feature selection. While wrapper methods often deliver better performance than filter methods by considering feature interactions, they generally require computationally expensive manual tuning [36]. ❸ Embedded methods integrate feature selection directly into the model training process, often leveraging regularization techniques to identify and select relevant features. A well-known example is the Least Absolute Shrinkage and Selection Operator (LASSO) [37], which enables input sparsification by adding a penalty as a coefficient on the model’s loss function. Although effective, LASSO struggles with multicollinearity and non-differentiable optimization.

B. Model Compression

Model compression techniques aim to reduce the computational and memory footprint of deep learning models without significantly compromising prediction accuracy [38]. This is crucial for deploying complex models on resource-constrained devices and for reducing latency in time-critical scientific applications.

On the algorithm side, the community has addressed the computational complexity in machine learning models by pruning redundant and unnecessary model parameters to improve efficiency at high accuracy. ❶ Unstructured pruning is individual weight pruning. For example, in a fully connected (FC) layer, unstructured pruning selectively removes certain weights, i.e., specific neuron connections with other layers. The importance of these connections determines their removal. For example, Lee et al. [39] proposed detecting insensitive weights using initialization conditions. The unstructured pruning, however, has a critical drawback: it may result in sparse weight matrices with removed connections represented by zeros, which cannot inherently lead to compression or speedup without specialized hardware or libraries [40].

Only a few leading semiconductor chips (such as NVIDIA A100/H100) have incorporated support for sparse operations. On hardware that lacks support for underlying sparse operators, which is commonly used by most domain scientists, the computation, such as sparse-dense matrix multiplication (SpMM), still operates in a dense (non-sparsified) manner. ❷ Structured pruning [41]–[43] operates at the level of channel, neuron, or even layer. For example, Li et al. [44] employ the $L1$ norm, while He et al. [45] use the $L2$ norm on the filter and weights to guide the model pruning. Structured pruning provides a systematic reduction (by removing rows or columns) of computation matrices, offering flexibility in machine learning layers and portability across hardware architectures. However, most structured methods suffer from inefficiencies in both algorithmic performance and tuning complexity. For instance, one of the representative approaches [46] relies on the hypothesis that “smaller norm-less-informative” requires an extra sensitivity analysis for verification. This sensitivity analysis is an iterative optimization process, which is time-consuming and prone to getting trapped in local optima. Instead of pruning a proportional part of the model, ❸ lightweight design [47], [48] and ❹ knowledge distillation [49], [50] compress the model by learning a new, smaller one. The lightweight design leverages a one-step training process, simplifying the tuning complexity but often sacrificing algorithmic performance [51]. Knowledge distillation uses an advanced teacher-student framework that enhances algorithm performance but requires careful design and domain expertise for both models.

On the system side, diverse high-performance architectures, such as NVIDIA GPUs, Intel CPUs, AMD GPUs, Cerebras, SambaNova, and Graphcore, have advanced alongside the rapid growth of large-scale machine learning models. Vendors like NVIDIA, beginning with the DGX-2 (Volta) in 2017, introduced Tensor Cores to enable mixed-precision and quantization computation, significantly reducing computational complexity and memory usage. The latest H200 architecture supports a broad range of precision formats, including FP64, FP32, FP16,

BF16, and INT8, and provides support for sparse matrix operations, further enhancing performance and efficiency. While hardware-specific optimizations for quantization are beyond the scope of this paper and are left for future work, our proposed framework, Lumos, offers a hardware-agnostic design for input and model sparsification. It can integrate with libraries across various architectures to explore and improve quantization efficiency.

In contrast to the above methods, our proposed framework, Lumos, automates and integrates input feature selection with model compression. Lumos is hardware-agnostic, ensuring portability across various hardware architectures; it is self-guided, requiring no human supervision during the model tuning process; and it is algorithm-efficient, offering fine-grained control over the trade-off between compression ratio and performance.

III. Design Overview

Figure 2 gives an overview of Lumos, an end-to-end framework to democratize feature selection, feature re-adaptation, and model architecture search (i.e., structure pruning with parameter optimization) for SciML models. Lumos aims to tackle the broad and fundamental implications of SciML models, such as convolutional neural network (CNN), multilayer perceptron (MLP), graph neural network (GNN) and Transformer [52], while meeting the requirements of time and cost efficiency. Given a basic model and its dataset from users, Lumos first applies gating parameters to each of the input features and model parameters (Section V). Specifically, Lumos adopts a semi-stochastic mechanism to regulate the initial states of the gates and applies a reparameterization function to make the gates differentiable within the backpropagation process.

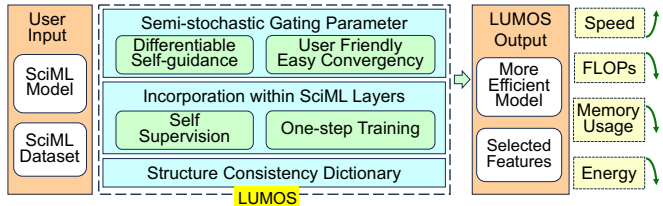


Fig. 2: Overall workflow of Lumos.

Then, Lumos incorporates the gates into SciML layers (Section VI). The cooperation regularizes the structured pruning on the vanilla structures of scientific inputs and SciML layers. Once integrated, the entire selection and optimization process in Lumos is a one-step training (in S1) or one-step fine-tuning (in S2), without user supervision or domain knowledge.

Next, with the sparsity indication of gates, Lumos incorporates a suite of structural alignment tools the Layer Consistency Mapper and the Special Structure Coordinator (Section VII) when conducting model distillation. These tools maintain architectural integrity and ensure

correct tensor alignment throughout the optimized model. After the above offline phase, Lumos produces an optimized model with the corresponding feature set, offering substantial improvements in computational and communication efficiency across latency, throughput, power, and storage in inference serving. Code is available on GitHub.¹

IV. Problem Formulation

A SciML model is fundamentally defined by two key components: model weights and input features (or feature datasets). The model weights are the learned parameters that constitute the trained model, typically organized across multiple layers. The input features (two examples are illustrated in Fig. 3) represent the input parameters or variables specific to the scientific application.

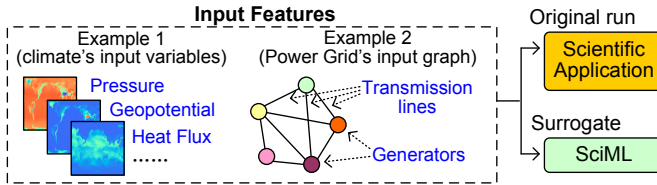


Fig. 3: Illustration of Input Features: the blue words represent input features regarding two examples, climate application and power grid simulation, respectively.

For a SciML model associated with weights and feature datasets, the optimization can be defined as follows (The symbols and notations are listed in Table I for reference throughout this paper):

TABLE I: Summary of Symbols

Symbol	Description
\mathcal{F}	SciML model
\mathcal{D}	Dataset
\mathbf{X}^0	Input features
$\mathbf{X}^{(l)}$	Input to the l -th layer
\mathbf{Y}^{gt}	Ground truth (output label)
\mathcal{M}	Set of evaluation metrics
l	Layer index
$\mathbf{H}^{(l+1)}$	Output of the l -th layer
$\mathbf{W}^{(l)}$	Weight matrix of the l -th layer
$m_j^{(l)}$	The i -th gating parameter of l -th layer
$\mathbf{b}^{(l)}$	Bias vector of the l -th layer
σ	Activation function
$g(\mathbf{X}^{(l)}, \mathbf{W}^{(l)})$	Layer-specific transformation function

Problem Formulation. Given a SciML model \mathcal{F} , a dataset $\mathcal{D} = (\mathbf{X}^0, \mathbf{Y}^{gt})$, and a set of evaluation metrics \mathcal{M} , the goal is to find an optimal subset of input features $\mathbf{X}' \subseteq \mathbf{X}^0$ and an optimized model $\mathcal{F}' \subseteq \mathcal{F}$ that reduces the total number of parameters (weights) while preserving accuracy. The optimization can be expressed as:

$$\arg \min_{\mathcal{F}' \subseteq \mathcal{F}, \mathbf{X}' \subseteq \mathbf{X}^0} |\mathcal{M}(\mathcal{F}(\mathbf{X}^0), \mathbf{Y}^{gt}) - \mathcal{M}(\mathcal{F}'(\mathbf{X}'), \mathbf{Y}^{gt})|,$$

where:

¹<https://github.com/Picomp-lab/Loxia>

- $\mathcal{F}(\mathbf{X}^0)$ denotes the output of the base model using the full set of input features \mathbf{X}^0 ;
- $\mathcal{F}'(\mathbf{X}')$ denotes the output of the optimized model along with the selected subset of features \mathbf{X}' .

V. Unifying Feature Selection and Model Compression

A. Semi-Stochastic Gating Parameters

We introduce semi-stochastic gating parameters that automatically optimize SciML models by applying differentiable neurons on both input and hidden layers, enabling efficient feature selection and model compression.

Each of the i -th gating parameter $m_i^{(l)}$ at l -th layer in the SciML model is associated with a gate, with a value $\pi_i^{(l)} \in [0, 1]$, which is represented in Equation (1). During training, $\pi_i^{(l)}$ is updated with the gradients of the loss function, dynamically adjusting the neuron's gating status, along with the optimization of SciML model parameters. After optimization, if $\pi_i^{(l)}$ exceeds the upper threshold t_u , the neuron remains active; if it falls below the lower threshold t_l , the neuron is deactivated and marked for removal along with the structural consistency tools described in Section VII. For values between t_l and t_u , the activation status is determined probabilistically using a Bernoulli distribution parameterized by $\pi_i^{(l)}$.

$$m_j^{(i)} = g(\pi_i^{(l)}) = \begin{cases} 1 & \pi_i^{(l)} > t_u, \\ \text{Bern}(\pi_i^{(l)}) & t_u \geq \pi_i^{(l)} > t_l, \\ 0 & t_l \geq \pi_i^{(l)}. \end{cases} \quad (1)$$

The approach of employing a threshold to regulate the gate's status is straightforward; however, its discrete nature makes an effective gradient-based optimization infeasible. In Sec V-B, we propose a method to approximate the gate in a differentiable manner to enhance optimization.

B. Reparametrization for Differentiable Optimization

To efficiently optimize gating parameters using gradient-based methods such as Adam [53] or SGD [54], we apply a reparameterization trick [55] that approximates the Bernoulli gate using a hard concrete function. Specifically, for the variable $m_j^{(i)}$ defined in Equation (1), we approximate it as follows:

$$\overset{\text{Randomly sampled seeds}}{\epsilon} \sim \text{uniform}(t_l, t_u) \quad \overset{\text{A temperature controller for smoothness}}{\tau} \quad \overset{\text{Learnable parameters}}{\alpha_j^{(i)}} \quad m_j^{(i)} = \sigma\left(\log \frac{\epsilon}{1 - \epsilon} + \alpha_j^{(i)}\right) / \tau, \quad (2)$$

where τ is the temperature parameter that controls the smoothness of the relaxation, and $\alpha_j^{(i)}$ is a learnable parameter. This formulation enables gradient propagation through the gating network, allowing simultaneous optimization of both the neuron weights (in the baseline SciML model) and the gate parameters (introduced by Lumos).

To further enhance differentiability, we adopt the hard-concrete relaxation [56], which stretches the output and clips its value within the range $[0, 1]$. Given the relaxed gating variable \tilde{m} (denoted as $\tilde{m}_j^{(i)}$ for clarity), we have:

$$\begin{aligned}
\tilde{m}_j^{(i)} &= \tilde{m}_j^{(i)}(\zeta - \gamma) + \gamma && \text{The scaling upper bound} \\
\tilde{m}_j^{(i)} &= \min(1, \max(0, \tilde{m}_j^{(i)})) && \text{The scaling lower bound} \\
&&& \text{Hard-Concrete regularization}
\end{aligned} \tag{3}$$

where $\gamma < 0$ and $\zeta > 1$ are hyperparameters that control the scaling and clipping behavior.

Now we add regularization to the cumulative density Q of the gating variable $\tilde{m}_j^{(i)}$, this optimization will lead the gating parameters to become 0 during the training process. The complexity loss, \mathcal{L}_C , which measures the SciML model's flexibility, is expressed as:

$$\mathcal{L}_C = \sum_{j=1}^{|\theta|} \left(1 - Q_{\tilde{m}_j^{(i)}}(0 | \phi) \right) \tag{4}$$

The parameters of the distribution are $\phi = (\log \alpha, \tau)$, where $\log \alpha$ is the location and τ is the temperature.

The complexity loss of the objective in Equation 4 under the hard concrete is equivalently expressed as follows:

$$\mathcal{L}_C = \sum_{j=1}^{|\theta|} \sigma \left(\log \alpha_j - \beta \log \left(-\frac{\gamma}{\zeta} \right) \right) \tag{5}$$

In summary, the total optimization is driven by two loss functions: a prediction loss and an additional regularization term \mathcal{L}_C that promotes the (de-)activation of neurons, determining the selection of input features and model parameters ultimately (with the implementation of structure coordination in Section VII). The combined loss function, \mathcal{L}_T , integrates both the accuracy loss (\mathcal{L}_A) and the complexity loss (\mathcal{L}_C) as follows:

$$\mathcal{L}_T = \mathcal{L}_A + \lambda \mathcal{L}_C, \tag{6}$$

where λ is a hyperparameter that balances \mathcal{L}_A and \mathcal{L}_C .

The overall optimization problem is then solved by minimizing the total loss \mathcal{L}_T , ensuring that both the model neurons and the distribution of gating parameters converge effectively.

VI. Incorporation within SciML Layers

We integrate gates at the input of each layer so that removing a gate deletes an entire input unit/channel and its fan-in weights. This yields structured sparsity, direct computation, and memory reduction.

Specifically, we apply element-wise gating parameters using the element-wise Hadamard product (\odot) to regulate the importance of different model components, while preserving the structural consistency of various neural network layers, such as fully connected, convolutional, graph-based, or attention layers (shown in Figure 4).

(1) Fully Connected (FC) Layer: The FC layer is one of the most widely used types in SciML models for regression problems. Structured pruning is applied to the FC layer,

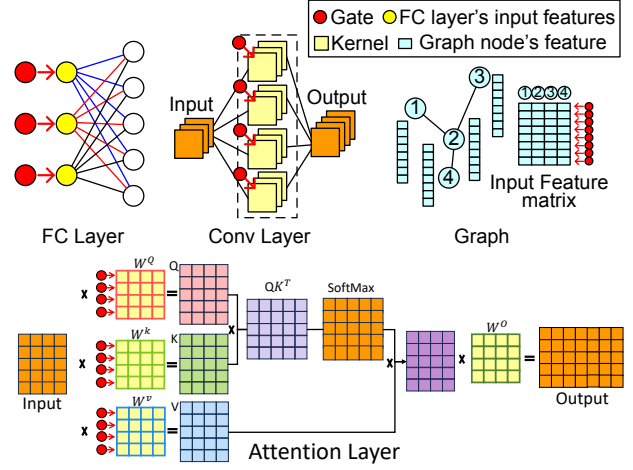


Fig. 4: Integration with different model layers.

with gating parameters focused on the row structure (input channels).

$$\mathbf{H}^{(l+1)} = \sigma \left(\mathbf{X}^{(l)} \cdot \mathbf{m}^{(l)} \odot \mathbf{W}^{(l)} + \mathbf{b}^{(l)} \right) \tag{7}$$

FC layers are ubiquitous in SciML models and form foundational components of CNNs, GINs, GCNs, and Transformers. We set the gating vector to match the number of rows (input units) in each FC layer, so that each gate modulates a group of FC weights. This design enables structured pruning in a principled, unit- or group-wise manner.

(2) Convolutional (CONV) Layer: The gating variables are integrated into the convolutional kernels depicted in yellow in Figure 4. The gating parameter $\mathbf{m}^{(l)} \in \mathbb{R}^{1 \times d}$ is applied to the output channels:

$$\mathbf{H}^{(l+1)} = \sigma \left(\text{conv}(\mathbf{X}^{(l)}, \mathbf{m}^{(l)} \odot \mathbf{W}^{(l)}) + \mathbf{b}^{(l)} \right) \tag{8}$$

(3) Graph Isomorphism Network (GIN) Layer: There are three stages in the GIN layer: embedding edge feature, aggregating neighboring nodes, and linearly map aggregated nodes. In the GIN layer, we applied the same gating parameters $\mathbf{m}^{(l)} \in \mathbb{R}^{1 \times n}$ to both the output of aggregation nodes and the input nodes to maintain the structure pruning consistency:

$$\mathbf{H}^{(l+1)} = \sigma \left(\mathbf{W}^{(l)} \left((1 + \epsilon) \cdot \mathbf{m}^{(l)} \odot \mathbf{X}^{(l)} + \mathbf{m}^{(l)} \odot \text{prop}(\text{emb}(\mathbf{E}), \mathbf{X}^{(l)}) \right) \right) \tag{9}$$

where:

- $\mathbf{E} \in \mathbb{R}^{1 \times e}$: Edge features, embedded to $\mathbb{R}^{e \times n}$.

(4) Graph Convolutional Network (GCN) Layer: A GCN layer [57] defines a first-order approximation of a localized spectral filter on graphs. GCNs can be understood as a

generalization of convolutional neural networks to graph-structured data. To keep structural consistency, we also apply the same gating parameters $\mathbf{m}^{(l)} \in \mathbb{R}^{1 \times n}$ to the input channels $\mathbf{W}_1^{(l)}$ and $\mathbf{W}_2^{(l)}$:

$$\begin{aligned} \mathbf{H}' &= \mathbf{W}_1^{(l)} \cdot \mathbf{X}^{(l)} + b_1^{(l)} \\ \mathbf{E}' &= \mathbf{W}_2^{(l)} \cdot \mathbf{E} + b_2^{(l)} \\ \mathbf{H}^{(l)} &= \mathbf{m}^{(l)} \odot \text{prop}(\mathbf{H}', \mathbf{E}') + \mathbf{m}^{(l)} \odot \text{ReLU}(\mathbf{H}' + \text{emb}(\mathbf{R})) \end{aligned} \quad \begin{array}{l} \text{Root node} \\ \downarrow \\ (10) \end{array}$$

↑ Transformed node features $\mathbb{R}^{m \times d}$ ↑ Transformed edge features $\mathbb{R}^{e \times d}$

(5) Attention Layer: For attention layers, gating parameters are applied to three input weight matrices: \mathbf{W}_Q , \mathbf{W}_K , and \mathbf{W}_V . All gating parameters are applied to the first dimension of weight matrices, as illustrated in Figure 4 and equations 11.

$$\begin{aligned} \mathbf{Q}^{(l)} &= \mathbf{X}^{(l)} \cdot \mathbf{m}_Q^{(l)} \odot \mathbf{W}_Q^{(l)} \\ \mathbf{K}^{(l)} &= \mathbf{X}^{(l)} \cdot \mathbf{m}_K^{(l)} \odot \mathbf{W}_K^{(l)} \\ \mathbf{V}^{(l)} &= \mathbf{X}^{(l)} \cdot \mathbf{m}_V^{(l)} \odot \mathbf{W}_V^{(l)} \\ \mathbf{H}^{(l+1)} &= \text{Attention}(\mathbf{Q}^{(l)}, \mathbf{K}^{(l)}, \mathbf{V}^{(l)}) \mathbf{W}_O^{(l)} \end{aligned} \quad (11)$$

↑ $\text{softmax}\left(\frac{\mathbf{Q}\mathbf{K}^T}{\sqrt{d}}\right) \mathbf{V}$

This gating mechanism can be seamlessly integrated into multi-head attention, enabling structured pruning while preserving the overall attention architecture.

VII. Structural Consistency

After the gate indication for neuron selection, the corresponding removal must maintain the remaining network executable: tensor dimensions must align, layer dependencies must hold, and model outputs must stay numerically valid. To guarantee these, we introduce a structural consistency mechanism that performs two core functions: (i) it tracks which channels, neurons, or features are preserved across layers, and (ii) it reconciles architectural transformations such as flattening, concatenation, or embedding, so that input-output mappings remain consistent.

A. Layer-Wise Consistency Mapping

Lumos maintains a consistency dictionary for each layer, composed of $[\text{input_mask}, \text{output_mask}]$ pairs. These masks encode the indices of preserved weights and propagate remove decisions across layers. The *input_mask* represents the indices of the input channels or neurons that are retained (those with gate values equal to ones). The *output_mask* represents the indices of the output channels. Below we present two representative mapping scenarios in Lumos.

1) Between the CONV and FC layer: In the transition from a CONV layer to an FC layer, the output of the CONV layer with spatial dimensions is flattened to serve as the input to the FC layer. We implement a function `CONV2FC_dictionary()` in Lumos for index-mapping. For example, as shown in Fig. 5, if the CONV layer contains weights $\mathbf{W} \in \mathbb{R}^{64 \times 128 \times 3 \times 3}$ and a pruning operation reduces the input channels from 64 to 50, the mapper adjusts the *output_mask* accordingly.²

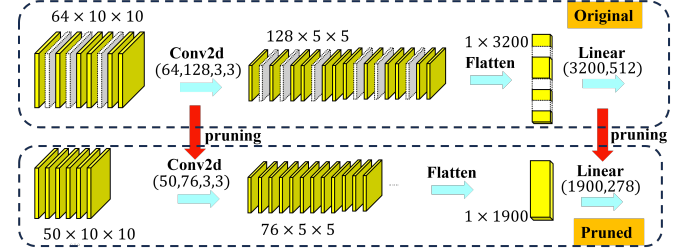


Fig. 5: Structured transition between the CONV and FC layer. When a CONV layer is followed by an FC layer, the output of the CONV layer serves as the input to the FC layer; therefore, the redundant outputs corresponding to the deactivated neurons of the CONV layer must also be removed to maintain tensor alignments.

2) Between the embedding and FC layer: In the transition from an embedding layer to a fully connected (FC) layer, the output vectors from the embedding layer serve as the input to the FC layer. In our design, gating parameters are applied only to the FC layer rather than directly to the embedding layer. To maintain structural consistency between these two layers, the embedding and FC layers share the same gating configuration. This means that when certain input channels of the FC layer are deactivated, the corresponding output dimensions of the embedding layer are also pruned to ensure proper tensor alignment.

As shown in Figure 6, we take a graph with five nodes and four edges as an example. Each node and edge is initially embedded into a 300-dimensional feature vector, resulting in a node embedding matrix of size 5×300 and an edge embedding matrix of size 4×300 . After Lumos optimizes the downstream FC layers, the gating mechanism identifies and removes redundant input channels, reducing the effective embedding dimensions to 189 for node features and 130 for edge features. Consequently, the corresponding FC layers are updated to accept inputs of sizes 189 and 130, respectively, maintaining structural alignment between the embedding and FC layers after optimization.

²The translation follows the equation of $\text{input_mask}[i] = \text{output_mask}[j] \times w \times h + k$, where w and h are the width and height of the output feature map from the CONV layer, and k is the specific position within each spatial dimension of the output feature map, ranging from 0 to $(w \times h - 1)$.

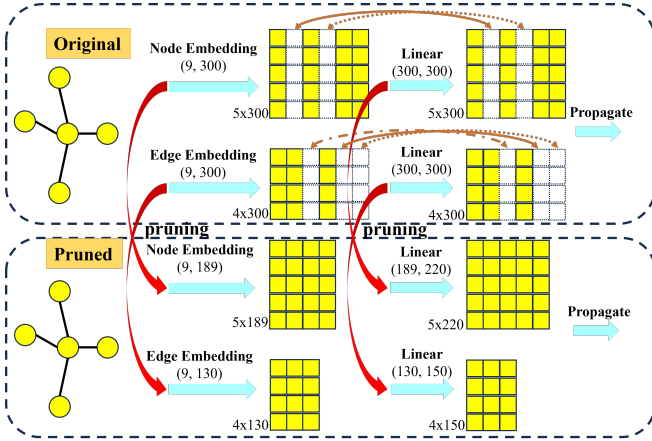


Fig. 6: Structured transition between the embedding and FC layer. When input features are deactivated, the corresponding weights in the following FC layer must also be removed.

B. Cross-Layer Topology Coordinator

When layers are concatenated, reshaped, or otherwise interconnected, maintaining consistent index alignment across them becomes non-trivial. The Topology Coordinator in Lumos addresses this challenge by systematically managing index mappings to ensure that optimization decisions, such as channel or neuron deactivation, are correctly propagated across dependent layers. This mechanism prevents tensor misalignment, preserves architectural integrity, and enables end-to-end structural optimization without user intervention.

Consider the case of concatenating two convolutional layers after optimization. As with flattening operations, it is essential to align the preserved indices in the respective dictionaries $\langle out_{mask_1}, out_{mask_2} \rangle$ with the in_{mask} of the downstream concatenated layer. In the example shown in Figure 7, the first convolutional layer reduces its output channels from 64 to 50, and the second from 64 to 47. After concatenation, the combined input to the subsequent layer consists of 97 channels instead of 128. The Topology Coordinator automatically merges the retained indices from both layers, applying the necessary offset to the second set to maintain correct ordering and ensure seamless connectivity.

Extracting consistent subnetworks from heterogeneous neural architectures is inherently complex. Lumos streamlines this process by encapsulating all required functionalities, including index mapping, mask propagation, and model extraction. Users only need to specify their model and dataset; Lumos autonomously manages the structural adjustments, delivering a compact, deployable model that preserves both functionality and layer connectivity.

C. Residual-Aware Layer Removal

Lumos can also remove redundant layers from a given model architecture. Figure 8 illustrates the pruning process applied inside a residual block. In the original structure (top), the residual branch contains an intermediate transformation layer (highlighted by the dashed box). During pruning, if all parameters of Layer2 or Layer3 are pruned by Lumos, then Block1 is identified as redundant and needs to be removed. Consequently, Lumos will directly connect the remaining blocks of the residual branch to the addition operation, while preserving compatibility with the skip connection.

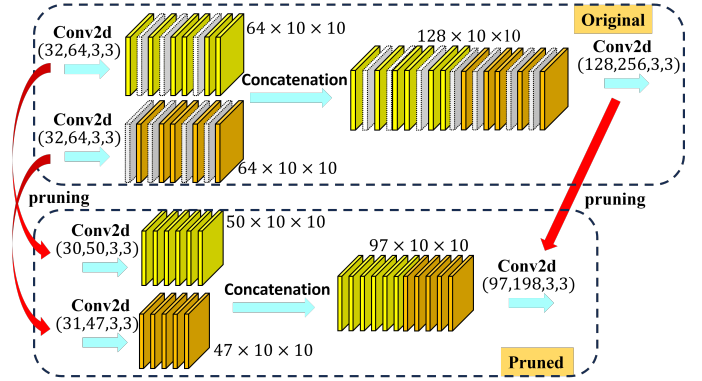


Fig. 7: Dependency between concatenation. When two outputs of two CONV layers are concatenated before being connected to another CONV layer, the indices of the CONV kernels must be remapped to maintain structural integrity.

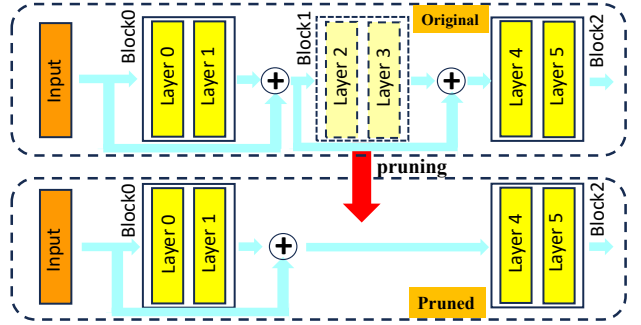


Fig. 8: Layer-wise pruning within a residual architecture.

transformation layer (highlighted by the dashed box). During pruning, if all parameters of Layer2 or Layer3 are pruned by Lumos, then Block1 is identified as redundant and needs to be removed. Consequently, Lumos will directly connect the remaining blocks of the residual branch to the addition operation, while preserving compatibility with the skip connection.

VIII. Performance Evaluation

Platform. All experiments are conducted on a computing cluster equipped with eight NVIDIA A100 GPUs, each with 80 GB of memory. The cluster is also powered by 96 Intel Xeon Gold 6342 CPU cores, operating at 2.80 GHz. The software environment includes CUDA version 12.3 and NVIDIA Driver version 545.23.08. Model training and inference are performed using Python 3.11 and PyTorch 2.2.

Workloads. Table II presents the diverse scientific workloads evaluated in this study. We assess the performance of Lumos across various applications, including fluid dynamics (CFD, Fluid), molecular dynamics (PureMD), cosmology (CosmoFlow), material science (DMS, EM-denoise, StemDL), physics (Optical, SLSTR), biology (PPA), chemistry (Molhiv), and medical science (Brain Tumor). These workloads feature a range of input modalities such as images, vectors, matrices, and graphs, as well as target tasks like regression and classification. To

better reflect the multi-sample, multi-iteration nature of SciML inference in real applications, we adopt dynamic batch size configurations³, with an upper bound of GPU memory usage for fair comparison.

TABLE II: Summary of evaluated scientific workloads

Workloads	Domain	Network	Task
CFD [59]	Fluid tion	Simula- FCs	Surrogate:Compute_Flux()
Fluid [59]	Fluid tion	Simula- FCs	Surrogate:Compute_Force()
Puremd [59]	Molecular	FCs	Surrogate:Add_dBond_to_Forces()
CosmFlow [60]	Cosmology	CONVs+FCs	Regression: The universe parameters
EM-DN [61]	Material Sciences	Unet	Regression: Denoising
Synthetic [61]	Math tion	formula- FCs	Regression: Math formulation
Optical [61]	Instrumentation	Enc.&Dec.	Detection: Optical equipment damage
DMS [61]	Material Sciences	CONVs+FCs	Classification: Image
STEM-DL [61]	Material Sciences	VGG	Classification: Diffraction patterns
SLSTR [61]	Atmospheric	Unet	Classification: Image(at pixel level)
PPA [62]	Biological Science	GCN	Classification: Taxonomic group
Molhiv [63]	Chemical Science	GIN	Classification: Molecular properties
BrainTumor [64]	Medical	ViT	Classification: Tumor detection

A. Overall Performance

We evaluate the overall performance of Lumos with four metrics: speedup (time-to-solution), accuracy, parameter reduction, and floating point operations (FLOPs). Each reflects a unique angle of Lumos’s efficiency.

① Speedup quantifies the reduction in inference time after applying Lumos. Figure 9a shows the end-to-end (E2E) latency improvements on two major hardware platforms: the NVIDIA A100 GPUs and Intel Xeon Gold 6342 CPUs. On GPUs, Lumos achieves up to a 51.6× speedup (CFD), with an average acceleration of 6.4× across all evaluated workloads. On CPUs, the speedup reaches 68.8× (CFD), averaging 7.6× overall. SciML workloads, particularly surrogate models, benefit significantly since their computational demands are linear with respect to model parameters. Even within architectures primarily featuring convolutional or graph operations, Lumos demonstrates measurable speedups while maintaining accuracy.

② Accuracy assesses the predictive quality of the optimized SciML models. We employ three standard metrics corresponding to the type of scientific task: Acc, R^2 score, and MSE. For classification-based SciML tasks, Acc measures the ratio of correctly predicted instances to the total number of samples, which is applied to the workloads of DMS, STEM-DL, Molhiv, Brain Tumor, and PPA. For regression-based SciML workloads, we employ the coefficient of determination (R^2) [65] to quantify how well the model explains the variance of the target variable: $R^2 = 1 - \frac{\sum_{i=1}^n (y_i - \hat{y}_i)^2}{\sum_{i=1}^n (y_i - \bar{y})^2}$. where \bar{y} denotes the

³A state-of-the-art (SOTA) evaluation strategy widely used to assess AI model efficiency, as demonstrated in works like ORCA [58].

mean of the ground-truth outputs. An R^2 value closer to 1 indicates stronger predictive fidelity. This metric is used for regression workloads, including CFD, PureMD, Fluid, and Synthetic. For continuous-valued prediction tasks emphasizing absolute accuracy, we adopt the mean squared error (MSE): $MSE = \frac{1}{n} \sum_{i=1}^n (y_i - \hat{y}_i)^2$ where lower values indicate higher precision. MSE is applied to workloads such as CosmoFlow, EM-Denoise, SLSTR, and Optical.

As shown in Figure 9b, Lumos generally preserves the predictive accuracy of the baseline SciML models and even improves performance in several cases. For regression workloads such as CosmoFlow, Optical, Synthetic, and PureMD, Lumos achieves modest accuracy gains while substantially reducing model parameters. Minor yet acceptable accuracy drops are observed in CFD (2.68%) and Fluid (0.52%). For classification workloads such as Brain Tumor and STEM-DL, the decrease is limited to 0.69–1.59%. Notably, Lumos alleviates overfitting in highly parameterized models; for instance, in DMS, it yields a clear accuracy improvement by regularizing redundant weights during training.

③ Effectiveness of Parameter Optimization. Figure 9c shows the parameter sizes before and after applying Lumos across all workloads. Lumos significantly reduces the number of active parameters from 37.4% (PPA) to 99.9% (CFD) with an average reduction ratio of 71.7%. These reductions result from adaptive gating that removes non-informative connections and dynamically reallocates model capacity during training. Importantly, the processed models remain structurally valid and executable, as verified by the consistency checking described in Section VII.

④ Floating-Point Operations (FLOPs). FLOPs quantify computational overhead and reflect the reduction in operational complexity. Figure 9d compares FLOPs before and after applying Lumos across all evaluated workloads. The baseline FLOPs range from 0.24 million (PureMD) to over 100 billion (STEM-DL), covering a wide variety of SciML architectures. Applying Lumos consistently lowers computational demand, achieving reductions from 6.3% (CosmoFlow) to 99.9% (CFD), with an average decrease of 69.6%. These results confirm that Lumos effectively minimizes redundant computations by jointly optimizing feature relevance and parameter utilization, thereby enhancing both efficiency and scalability.

B. Comparison with Other SoTA Model Compression Methods

We compare Lumos against four representative frameworks from the four categories of state-of-the-art model optimization methods discussed in Section II-B: (1) Only Train Once (OTO) [66], (2) L1-norm regularization (L1) [44], (3) NEURAL [67], and (4) DepGraph [68]. We evaluate all methods across five representative workloads, including PureMD, CFD, EM-Denoise, DMS, and Brain

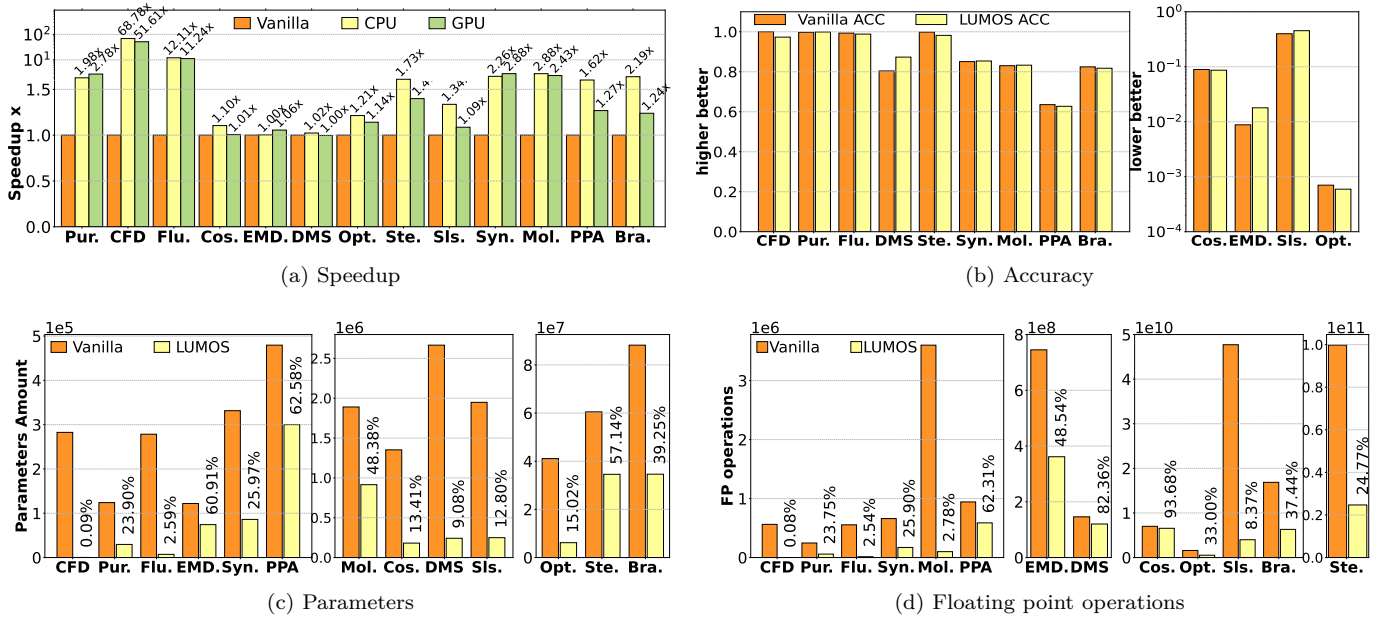


Fig. 9: Comparison between baseline SciML models and Lumos across latency, accuracy, parameter count, and FLOPs.

TABLE III: Comparison with SOTA pruning methods

Metrics	OTO	L1	NEURAL	DepGraph	Lumos
One-Shot	Yes	No	No	Yes	Yes
Compression	Yes	Yes	No	Yes	Yes
Adaptiveness	No	No	No	No	Yes
Puremd(% \uparrow)	72.73%	76.3%	80.10%	76.35%	76.10%
Puremd($R^2\uparrow$)	0.9430	0.9969	0.9318	0.9937	0.9988
CFD(% \uparrow)	99.10%	99.12%	99.10%	99.12%	99.10%
CFD($R^2\uparrow$)	0.5933	0.9136	0.9785	0.9747	0.9732
EMD.(% \uparrow)	30.10%	39.30%	39.50%	39.33%	39.09%
EMD.(MSE \downarrow)	9.13e-3	0.0401	0.021	0.041	9.51e-3
DMS.(% \uparrow)	91.00%	91.02%	91.09%	91.22%	90.92%
DMS.(ACC \uparrow)	67.35	75.94	72.06	71.11%	87.33
Bra.(% \uparrow)	60.34%	59.98%	61.09%	-	60.75%
Bra.(ACC \uparrow)	78.41	80.94	79.06	-	81.77

Note: ' \uparrow ' indicates that higher is better; ' \downarrow ' indicates that lower is better; '-' indicates that the latest version can't support this application.

Tumor. These workloads cover the five-layer types described in Section VI. We assess performance using both the parameter reduction ratio, listed in the first row, and accuracy metrics (R^2 , classification accuracy(Acc), and MSE depending on each task's objective) shown in the second row of each evaluated workload.

As shown in Table III, Lumos performs consistently well across all evaluated workloads and metrics. Compared with OTO, L1, NEURAL, and DepGraph, Lumos achieves competitive or higher accuracy while maintaining strong compression efficiency. For regression tasks such as PureMD and CFD, Lumos reaches the highest R^2 scores (0.9988 and 0.9732) with similar or fewer parameters than other methods. In the EM-Denoise task, it records the lowest mean squared error (9.51×10^{-3}), indicating more precise predictions. For classification tasks such as DMS and Brain Tumor, Lumos also achieves high accuracy (87.33% and 81.77%), comparable to or better

than existing methods. These results show that Lumos can effectively balance model size and prediction quality, providing a simple and adaptive approach that works well across different SciML architectures.

C. Feature Selection Analysis

We evaluate Lumos's feature selection capability using three representative surrogate models, i.e., CFD, PureMD, and Fluid. Each SciML model is trained on a distinct physical simulation (Figure 10), where the input-output data dependencies are analyzed and identified by a compiler-based framework [69]. These tasks consist of numerical input arrays with complex inter-feature relationships, making them well-suited for assessing Lumos's effectiveness in selecting the most informative and relevant features.

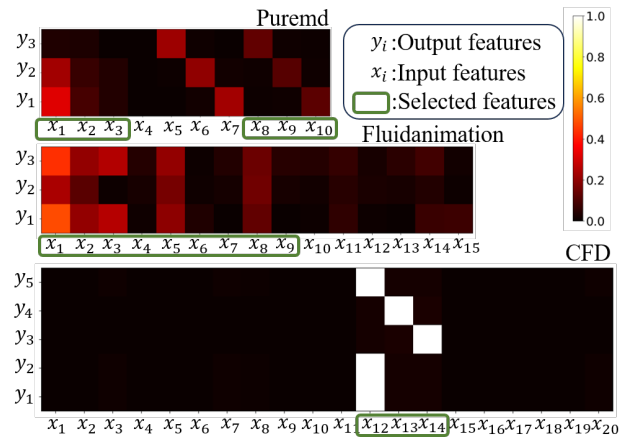


Fig. 10: Showcase I: Feature selection efficiency in three regression workloads (CFD, PureMD, and Fluid).

To quantify feature relevance, we use the Pearson

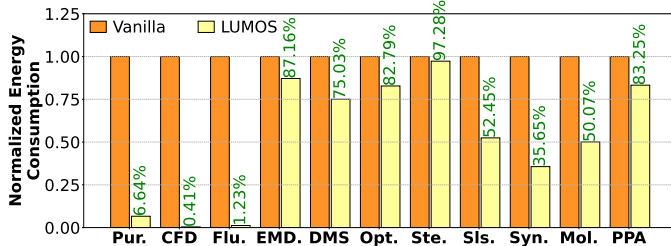
correlation coefficient to measure the linear relationship between each input variable \mathbf{x} and output variable \mathbf{y} :

$$\rho(\mathbf{x}, \mathbf{y}) = \frac{\text{Cov}(\mathbf{x}, \mathbf{y})}{\sigma(\mathbf{x})\sigma(\mathbf{y})}, \quad (12)$$

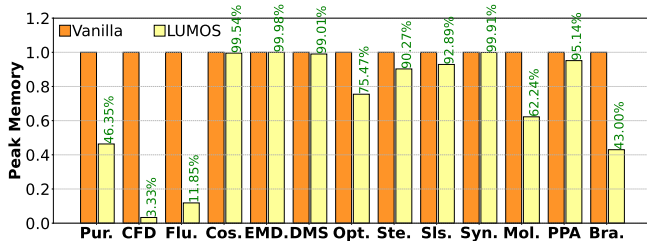
where Cov denotes covariance and $\sigma(\cdot)$ represents the standard deviation. A larger absolute value of ρ indicates a stronger linear dependency between the input and output variables.

As shown in Figure 10, Lumos consistently identifies the input dimensions that exhibit the highest correlations with their corresponding outputs. For instance, in the CFD model, Lumos automatically selects three key input features x_{12}, x_{13}, x_{14} that are most correlated with the target outputs y_1, \dots, y_5 , while suppressing inputs with negligible correlation ($|\rho| \approx 0$). Similarly, in the PureMD and Fluid models, the selected features align with the dominant physical variables governing system behavior, demonstrating the interpretability and reliability of Lumos’s gating-based feature optimization. These results confirm that Lumos effectively identifies and retains scientifically meaningful features while eliminating redundant or weakly relevant inputs.

D. Peak Memory Usage and Energy Saving



(a) Energy consumption



(b) Memory usage

Fig. 11: Peak Memory Usage and Energy Saving.

Energy Consumption quantifies power usage, providing an additional perspective on Lumos’s operational and environmental efficiency. Figure 11a presents the energy measurements obtained using a state-of-the-art power profiling tool [70]. On average, Lumos reduces energy consumption by 50.7% across all evaluated workloads. For compact, FC layer-dominant models such as PureMD, CFD, and Fluid, energy savings exceed 90%, highlighting the strong correlation between reduced computational cost and lower power demand. Moderate yet consistent

reductions of 30–60% are also observed in image- and graph-based workloads, including SLSTR, Synthetic, and Molhiv.

Peak Memory Usage measures the maximum memory consumption during execution. Figure 11b shows the reduction in peak memory achieved by Lumos. Across all workloads, Lumos reduces memory usage by up to 96.7%. The largest savings are observed in compact models such as PureMD, CFD, and Fluid, with reductions of 555 MB, 988 MB, and 914 MB, respectively. In larger convolutional architectures, memory savings are smaller because intermediate activation tensors in CONV layers dominate memory consumption and are less affected by feature or parameter optimization. Even so, Lumos effectively reduces both activation and weight footprints, allowing larger batch sizes and higher throughput during training and inference.

E. Scalability and Training Convergence

Scalability Analysis. Figure 12 illustrates the scalability of Lumos compared to the original training approach across four different models: Cosmoflow, Stemdl, Slstr, and Optical. All experiments were conducted using Distributed Data Parallel (DDP) training on up to 8 NVIDIA V100 GPUs (32GB each). Each model was trained for 200 epochs to ensure convergence, with batch size per GPU kept constant across different node counts for fair comparison.

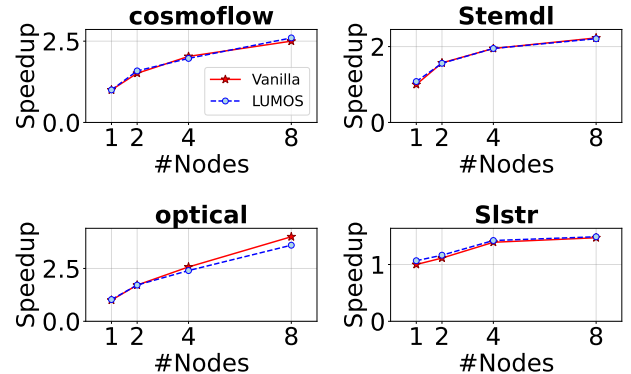


Fig. 12: Scale Lumos up to 8 GPUs using DDP training.

The results show that Lumos-integrated training has nearly the same scalability as vanilla training. Lumos introduces no observable scalability bottlenecks, as it adds lightweight gating parameters to each neuron without modifying the model’s architecture or communication pattern. On average, these additional gates account for only about 3% of the total parameters across the 13 evaluated models, imposing negligible overhead and remaining fully compatible with standard DDP training.

Training Convergence. Figure 13 shows the convergence behavior of the baseline and Lumos-optimized models over 200,000 training steps. Throughout training, Lumos consistently achieves lower loss values than the baseline.

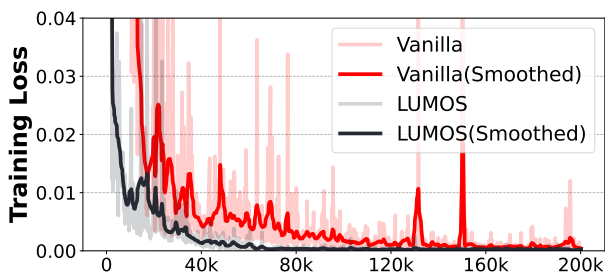


Fig. 13: Showcase II: Training loss over time for the baseline and Lumos-augmented models on the PureMD workload. Lumos achieves faster convergence, lower final loss, and greater training stability compared with the baseline training process.

The smoothed optimized loss curve (black) descends more rapidly and stabilizes at a lower final value than the smoothed baseline curve (red), demonstrating faster convergence and improved training stability.

TABLE IV: Training-time(minutes) overhead of integrating LUMOS.

Workload	Original	LUMOS	Overhead
cifar10	55	61	+10.91%
DMSNet	80	82	+2.50%
PPA	128	137	+7.03%
Molhiv	43	41	-4.65%
Slstr	129	131	+1.55%
CFD	34	37	+8.82%

Training Overhead. Table IV reports the training-time overhead introduced by LUMOS across representative workloads. Overall, the preliminary results indicate that LUMOS incurs only a modest overhead (below 11%), which is expected: the semi-stochastic gates introduce a small fraction of additional learnable parameters and only lightweight, element-wise computations, while being optimized jointly within a single end-to-end training run. In contrast, typical pruning baselines (e.g., iterative magnitude pruning or multi-round structured pruning) often require repeated prune-and-retrain cycles, leading to substantially higher wall-clock costs. Taken together, LUMOS preserves near-vanilla training cost, consistent with the same tendency observed in our broader experiments.

IX. Conclusion

Lumos is a comprehensive end-to-end framework that unifies input feature selection, model sparsification, and structured model extraction for SciML workloads. By leveraging semi-stochastic gating, Lumos integrates feature selection and parameter optimization directly into the training process while remaining fully compatible with standard SciML layer types. Designed to be hardware-agnostic and easy to integrate, Lumos enables researchers to deploy efficient models in resource-constrained environments without compromising accuracy. Extensive evaluations across 13 diverse scientific applications show that Lumos significantly reduces FLOPs, inference latency, memory footprint, and energy consumption, providing a

practical and scalable solution for next-generation scientific machine learning construction pipelines.

X. Acknowledgment

This work is supported by the U.S. National Science Foundation (2514351 and 2505118), and also supported by the U.S. Department of Energy, Office of Science, Advanced Scientific Computing Research (ASCR), under contracts DE-AC02-06CH11357. We thank the anonymous reviewers for their valuable feedback.

References

- [1] Andreas S. Panayides, Amir Amini, Nenad D. Filipovic, Ashish Sharma, Sotirios A. Tsaftaris, Alistair Young, David Foran, Nhan Do, Spyretta Golemati, Tahsin Kurc, Kun Huang, Konstantina S. Nikita, Ben P. Veasey, Michalis Zervakis, Joel H. Saltz, and Constantinos S. Pattichis. Ai in medical imaging informatics: Current challenges and future directions. *IEEE Journal of Biomedical and Health Informatics*, 24(7):1837–1857, 2020.
- [2] Alexander Brace, Igor Yakushin, Heng Ma, Anda Trifan, Todd Munson, Ian Foster, Arvind Ramanathan, Hyungro Lee, Matteo Turilli, and Shantenu Jha. Coupling streaming ai and hpc ensembles to achieve 100–1000× faster biomolecular simulations. In *2022 IEEE International Parallel and Distributed Processing Symposium (IPDPS)*, pages 806–816. IEEE, 2022.
- [3] Austin Clyde, Xuefeng Liu, Thomas Brettin, Hyunseung Yoo, Alexander Partin, Yadu Babuji, Ben Blaiszik, Jamaludin Mohd-Yusof, Andre Merzky, Matteo Turilli, Shantenu Jha, Arvind Ramanathan, and Rick Stevens. Ai-accelerated protein-ligand docking for sars-cov-2 is 100-fold faster with no significant change in detection. *Scientific Reports*, 13(1):2105, 2023.
- [4] Stephan Rasp, Michael S Pritchard, and Pierre Gentine. Deep learning to represent subgrid processes in climate models. *Proceedings of the national academy of sciences*, 115(39):9684–9689, 2018.
- [5] Gökcen Eraslan, Lukas M Simon, Maria Mircea, Nikola S Mueller, and Fabian J Theis. Single-cell rna-seq denoising using a deep count autoencoder. *Nature communications*, 10(1):390, 2019.
- [6] Jonathan M Stokes, Kevin Yang, Kyle Swanson, Wengong Jin, Andres Cubillos-Ruiz, Nina M Donghia, Craig R MacNair, Shawn French, Lindsey A Carfrae, Zohar Bloom-Ackermann, et al. A deep learning approach to antibiotic discovery. *Cell*, 180(4):688–702, 2020.
- [7] Dev Desai, Shiv V Kantliwala, Jyothi Vybhavi, Renju Ravi, Harshkumar Patel, Jitendra Patel, and RENJU RAVI. Review of alphafold 3: transformative advances in drug design and therapeutics. *Cureus*, 16(7), 2024.
- [8] Xiaozhe Ren, Pingyi Zhou, Xinfan Meng, Xinjing Huang, Yadao Wang, Weichao Wang, Pengfei Li, Xiaoda Zhang, Alexander Podolskiy, Grigory Arshinov, et al. Pangu- $\{\Sigma\}$: Towards trillion parameter language model with sparse heterogeneous computing. *arXiv preprint arXiv:2303.10845*, 2023.
- [9] Tung Nguyen, Johannes Brandstetter, Ashish Kapoor, Jayesh K Gupta, and Aditya Grover. Climax: A foundation model for weather and climate. *arXiv preprint arXiv:2301.10343*, 2023.
- [10] Zhuoran Qiao, Weili Nie, Arash Vahdat, Thomas F Miller III, and Animashree Anandkumar. State-specific protein-ligand complex structure prediction with a multiscale deep generative model. *Nature Machine Intelligence*, 6(2):195–208, 2024.
- [11] Shuya Nakata, Yoshiharu Mori, and Shigenori Tanaka. End-to-end protein-ligand complex structure generation with diffusion-based generative models. *BMC bioinformatics*, 24(1):233, 2023.
- [12] Minkyung Baek, Ryan McHugh, Ivan Anishchenko, Hanlun Jiang, David Baker, and Frank DiMaio. Accurate prediction of protein-nucleic acid complexes using rosettafoldna. *Nature methods*, 21(1):117–121, 2024.

- [13] Raphael JL Townshend, Stephan Eismann, Andrew M Watkins, Ramya Rangan, Masha Karelina, Rhiju Das, and Ron O Dror. Geometric deep learning of rna structure. *Science*, 373(6558):1047–1051, 2021.
- [14] Dejun Jiang, Chang-Yu Hsieh, Zhenxing Wu, Yu Kang, Jike Wang, Ercheng Wang, Ben Liao, Chao Shen, Lei Xu, and Jian Wu. Interactiongraphnet: A novel and efficient deep graph representation learning framework for accurate protein–ligand interaction predictions. *Journal of medicinal chemistry*, 64(24):18209–18232, 2021.
- [15] Huaipan Jiang, Jian Wang, Weilin Cong, Yihe Huang, Morteza Ramezani, Anup Sarma, Nikolay V Dokholyan, Mehrdad Mahdavi, and Mahmut T Kandemir. Predicting protein–ligand docking structure with graph neural network. *Journal of chemical information and modeling*, 62(12):2923–2932, 2022.
- [16] Gabriele Corso, Hannes Stärk, Bowen Jing, Regina Barzilay, and Tommi Jaakkola. Diffdock: Diffusion steps, twists, and turns for molecular docking. arXiv preprint arXiv:2210.01776, 2022.
- [17] Hannes Stärk, Octavian Ganea, Lagnajit Pattanaik, Regina Barzilay, and Tommi Jaakkola. Equibind: Geometric deep learning for drug binding structure prediction. In International conference on machine learning, pages 20503–20521. PMLR, 2022.
- [18] Zhirui Liao, Ronghui You, Xiaodi Huang, Xiaojun Yao, Tao Huang, and Shanfeng Zhu. Deepdock: enhancing ligand-protein interaction prediction by a combination of ligand and structure information. In 2019 IEEE International Conference on Bioinformatics and Biomedicine (BIBM), pages 311–317. IEEE, 2019.
- [19] Wei Lu, Qifeng Wu, Jixian Zhang, Jiahua Rao, Chengtao Li, and Shuangjia Zheng. Tankbind: Trigonometry-aware neural networks for drug-protein binding structure prediction. *Advances in neural information processing systems*, 35:7236–7249, 2022.
- [20] Gengmo Zhou, Zhifeng Gao, Qiankun Ding, Hang Zheng, Hongteng Xu, Zhewei Wei, Linfeng Zhang, and Guolin Ke. Unimol: A universal 3d molecular representation learning framework. 2023.
- [21] Tao Shen, Zhihang Hu, Zhangzhi Peng, Jiayang Chen, Peng Xiong, Liang Hong, Liangzhen Zheng, Yixuan Wang, Irwin King, and Sheng Wang. E2efold-3d: end-to-end deep learning method for accurate de novo rna 3d structure prediction. arXiv preprint arXiv:2207.01586, 2022.
- [22] Marc van Dijk and Alexandre MJJ Bonvin. Pushing the limits of what is achievable in protein–dna docking: benchmarking haddock’s performance. *Nucleic acids research*, 38(17):5634–5647, 2010.
- [23] Rohit K Tripathy and Ilias Bilionis. Deep uq: Learning deep neural network surrogate models for high dimensional uncertainty quantification. *Journal of computational physics*, 375:565–588, 2018.
- [24] Wenqian Dong, Gokcen Kestor, and Dong Li. Auto-hpcnet: An automatic framework to build neural network-based surrogate for high-performance computing applications. In Proceedings of the ACM International Symposium on High-Performance Parallel and Distributed Computing (HPDC ’23). ACM, 2023.
- [25] Ning Wang, Yang Gao, Hao Chen, Peng Wang, Zhi Tian, Chunhua Shen, and Yanning Zhang. Nas-fcos: Fast neural architecture search for object detection. In proceedings of the IEEE/CVF conference on computer vision and pattern recognition, pages 11943–11951, 2020.
- [26] Pierre Baldi, Peter Sadowski, and Daniel Whiteson. Searching for exotic particles in high-energy physics with deep learning. *Nature communications*, 5(1):4308, 2014.
- [27] Girish Chandrashekar and Ferat Sahin. A survey on feature selection methods. *Computers & electrical engineering*, 40(1):16–28, 2014.
- [28] Hanchuan Peng, Fuhui Long, and Chris Ding. Feature selection based on mutual information criteria of max-dependency, max-relevance, and min-redundancy. *IEEE Transactions on pattern analysis and machine intelligence*, 27(8):1226–1238, 2005.
- [29] Jacek Biesiada and Włodzisław Duch. Feature selection for high-dimensional data—a pearson redundancy based filter. In *Computer recognition systems 2*, pages 242–249. Springer, 2008.
- [30] Xin Jin, Anbang Xu, Rongfang Bie, and Ping Guo. Machine learning techniques and chi-square feature selection for cancer classification using sage gene expression profiles. In *Data Mining for Biomedical Applications: PAKDD 2006 Workshop, BioDM 2006*, Singapore, April 9, 2006. Proceedings, pages 106–115. Springer, 2006.
- [31] Nguyen Duc Thang, Young-Koo Lee, et al. An improved maximum relevance and minimum redundancy feature selection algorithm based on normalized mutual information. In 2010 10th IEEE/IPSJ International Symposium on Applications and the Internet, pages 395–398. IEEE, 2010.
- [32] Firuz Kamalov, Said Elnaffar, Aswani Cherukuri, and Annapurna Jonnalagadda. Forward feature selection: empirical analysis. *Journal of Intelligent Systems and Internet of Things*, 11(1):44–54, 2024.
- [33] Jeonghwan Park, Kang Li, and Huiyu Zhou. K-fold subsampling based sequential backward feature elimination. arXiv preprint arXiv:2503.11919, 2025.
- [34] Nicholas Pudjihartono, Tayaza Fadason, Andreas W Kempa-Liehr, and Justin M O’Sullivan. A review of feature selection methods for machine learning-based disease risk prediction. *Frontiers in bioinformatics*, 2:927312, 2022.
- [35] Vasileios Ch Korfiatis, Pantelis A Asvestas, Konstantinos K Delibasis, and George K Matsopoulos. A classification system based on a new wrapper feature selection algorithm for the diagnosis of primary and secondary polycythemia. *Computers in biology and medicine*, 43(12):2118–2126, 2013.
- [36] Isabelle Guyon and André Elisseeff. An introduction to variable and feature selection. *Journal of Machine Learning Research*, 3:1157–1182, 2003.
- [37] Robert Tibshirani. Regression shrinkage and selection via the lasso. *Journal of the Royal Statistical Society Series B: Statistical Methodology*, 58(1):267–288, 1996.
- [38] Yu Cheng, Duo Wang, Pan Zhou, and Tao Zhang. A survey of model compression and acceleration for deep neural networks. arXiv preprint arXiv:1710.09282, 2017.
- [39] Namhoon Lee, Thalaisyngam Ajanthan, Stephen Gould, and Philip HS Torr. A signal propagation perspective for pruning neural networks at initialization. arXiv preprint arXiv:1906.06307, 2019.
- [40] Aojun Zhou, Yukun Ma, Junnan Zhu, Jianbo Liu, Zhijie Zhang, Kun Yuan, Wenxiu Sun, and Hongsheng Li. Learning n: m fine-grained structured sparse neural networks from scratch. arXiv preprint arXiv:2102.04010, 2021.
- [41] Xiaohan Ding, Guiguang Ding, Yuchen Guo, and Jungong Han. Centripetal sgd for pruning very deep convolutional networks with complicated structure. In Proceedings of the IEEE/CVF conference on computer vision and pattern recognition, pages 4943–4953, 2019.
- [42] Liyang Liu, Shilong Zhang, Zhanghui Kuang, Aojun Zhou, Jing-Hao Xue, Xinjiang Wang, Yimin Chen, Wenming Yang, Qingmin Liao, and Wayne Zhang. Group fisher pruning for practical network compression. In International Conference on Machine Learning, pages 7021–7032. PMLR, 2021.
- [43] Zhonghui You, Kun Yan, Jinmian Ye, Meng Ma, and Ping Wang. Gate decorator: Global filter pruning method for accelerating deep convolutional neural networks. *Advances in neural information processing systems*, 32, 2019.
- [44] Hao Li, Asim Kadav, Igor Durdanovic, Hanan Samet, and Hans Peter Graf. Pruning filters for efficient convnets. arXiv preprint arXiv:1608.08710, 2016.
- [45] Yang He, Guoliang Kang, Xuanyi Dong, Yanwei Fu, and Yi Yang. Soft filter pruning for accelerating deep convolutional neural networks. arXiv preprint arXiv:1808.06866, 2018.
- [46] Jianbo Ye, Xin Lu, Zhe Lin, and James Z Wang. Rethinking the smaller-norm-less-informative assumption in channel pruning of convolution layers. arXiv preprint arXiv:1802.00124, 2018.
- [47] Forrest N Iandola, Song Han, Matthew W Moskewicz, Khalid Ashraf, William J Dally, and Kurt Keutzer. Squeezenet: Alexnet-level accuracy with 50x fewer parameters and < 0.5 mb model size. arXiv preprint arXiv:1602.07360, 2016.
- [48] Andrew G Howard, Menglong Zhu, Bo Chen, Dmitry Kalenichenko, Weijun Wang, Tobias Weyand, Marco Andreetto, and Hartwig Adam. Mobilenets: Efficient convolutional neu-

- ral networks for mobile vision applications. arXiv preprint arXiv:1704.04861, 2017.
- [49] Lu Yu, Vacit Oguz Yazici, Xialei Liu, Joost van de Weijer, Yongmei Cheng, and Arnau Ramisa. Learning metrics from teachers: Compact networks for image embedding. In Proceedings of the IEEE/CVF Conference on Computer Vision and Pattern Recognition, pages 2907–2916, 2019.
- [50] Frederick Tung and Greg Mori. Similarity-preserving knowledge distillation. In Proceedings of the IEEE/CVF international conference on computer vision, pages 1365–1374, 2019.
- [51] Zhuo Li, Hengyi Li, and Lin Meng. Model compression for deep neural networks: A survey. *Computers*, 12(3):60, 2023.
- [52] Ashish Vaswani, Noam Shazeer, Niki Parmar, Jakob Uszkoreit, Llion Jones, Aidan N Gomez, Łukasz Kaiser, and Illia Polosukhin. Attention is all you need. *Advances in neural information processing systems*, 30, 2017.
- [53] Diederik P Kingma and Jimmy Ba. Adam: A method for stochastic optimization. arXiv preprint arXiv:1412.6980, 2014.
- [54] Herbert Robbins and Sutton Monro. A stochastic approximation method. *The annals of mathematical statistics*, pages 400–407, 1951.
- [55] Christos Louizos, Max Welling, and Diederik P. Kingma. Learning sparse neural networks through l_0 regularization. In International Conference on Learning Representations, 2018.
- [56] Christos Louizos, Max Welling, and Diederik P Kingma. Learning sparse neural networks through l_0 regularization. arXiv preprint arXiv:1712.01312, 2017.
- [57] Thomas N Kipf and Max Welling. Semi-supervised classification with graph convolutional networks. arXiv preprint arXiv:1609.02907, 2016.
- [58] Gyeong-In Yu, Joo Seong Jeong, Geon-Woo Kim, Soojeong Kim, and Byung-Gon Chun. Orca: A distributed serving system for Transformer-Based generative models. In 16th USENIX Symposium on Operating Systems Design and Implementation (OSDI 22), pages 521–538, Carlsbad, CA, July 2022. USENIX Association.
- [59] Wenqian Dong, Gokcen Kestor, and Dong Li. Auto-hpcnet: An automatic framework to build neural network-based surrogate for high-performance computing applications. In Proceedings of the 32nd International Symposium on High-Performance Parallel and Distributed Computing, pages 31–44, 2023.
- [60] Amrita Mathuriya, Deborah Bard, Peter Mendygral, Lawrence Meadows, James Arnemann, Lei Shao, Siyu He, Tuomas Kärnä, Diana Moise, and Simon J Pennycook. Cosmoflow: Using deep learning to learn the universe at scale. In SC18: International Conference for High Performance Computing, Networking, Storage and Analysis, pages 819–829. IEEE, 2018.
- [61] Jeyan Thiyagalingam, Mallikarjun Shankar, Geoffrey Fox, and Tony Hey. Scientific machine learning benchmarks. *Nature Reviews Physics*, 4(6):413–420, 2022.
- [62] Damian Szklarczyk, Annika L Gable, David Lyon, Alexander Junge, Stefan Wyder, Jaime Huerta-Cepas, Milan Simonovic, Nadezhda T Doncheva, John H Morris, Peer Bork, et al. String v11: protein–protein association networks with increased coverage, supporting functional discovery in genome-wide experimental datasets. *Nucleic acids research*, 47(D1):D607–D613, 2019.
- [63] Zhenqin Wu, Bharath Ramsundar, Evan N Feinberg, Joseph Gomes, Caleb Geniesse, Aneesh S Pappu, Karl Leswing, and Vijay Pande. Moleculenet: a benchmark for molecular machine learning. *Chemical science*, 9(2):513–530, 2018.
- [64] Kaynaaf. Brain-tumour mri dataset. <https://huggingface.co/datasets/Kaynaaf/Brain-Tumour-MRI>, 2023. Accessed: YYYY-MM-DD.
- [65] RG Carpenter. Principles and procedures of statistics, with special reference to the biological sciences. *The Eugenics Review*, 52(3):172, 1960.
- [66] Tianyi Chen, Bo Ji, Tianyu Ding, Biyi Fang, Guanyi Wang, Zhihui Zhu, Luming Liang, Yixin Shi, Sheng Yi, and Xiao Tu. Only train once: A one-shot neural network training and pruning framework. *Advances in Neural Information Processing Systems*, 34:19637–19651, 2021.
- [67] Zhuang Liu, Jianguo Li, Zhiqiang Shen, Gao Huang, Shoumeng Yan, and Changshui Zhang. Learning efficient convolutional networks through network slimming. In Proceedings of the IEEE international conference on computer vision, pages 2736–2744, 2017.
- [68] Gongfan Fang, Xinyin Ma, Mingli Song, Michael Bi Mi, and Xinchao Wang. Depgraph: Towards any structural pruning. In Proceedings of the IEEE/CVF Conference on Computer Vision and Pattern Recognition, pages 16091–16101, 2023.
- [69] Zane Fink, Konstantinos Parasyris, Praneet Rathi, Giorgis Georgakoudis, Harshitha Menon, and Peer-Timo Bremer. Hpacml: A programming model for embedding ml surrogates in scientific applications. In SC24: International Conference for High Performance Computing, Networking, Storage and Analysis, pages 1–16. IEEE, 2024.
- [70] Xiaolong Tu, Anik Mallik, Dawei Chen, Kyungtae Han, Onur Altintas, Haoxin Wang, and Jiang Xie. Unveiling energy efficiency in deep learning: Measurement, prediction, and scoring across edge devices. In 2023 IEEE/ACM Symposium on Edge Computing (SEC), pages 80–93. IEEE, 2023.